

# SCIENTIFIC REPORTS

OPEN

## Differential binding affinity of tau repeat region R2 with neuronal-specific $\beta$ -tubulin isotypes

Vishwambhar Vishnu Bhandare, Bajarang Vasant Kumbhar & Ambarish Kunwar 

Tau is a microtubule-associated protein whose C-terminal domain consisting of four repeat regions R1, R2, R3 and R4 binds to microtubules to stabilize them. In several neurodegenerative diseases, tau detaches from microtubules to form insoluble aggregates leading to tauopathy. Microtubules are made up of  $\alpha\beta$  tubulin subunits. Seven  $\alpha$ -tubulin and nine  $\beta$ -tubulin isotypes have been reported to be present in humans till date. These tubulin isotypes show residue composition variations mainly at C-terminal region and bind to motor proteins and anti-mitotic drugs differently. These tubulin isotypes show tissue specific expression as their relative proportion varies significantly in different type of cells. It is also known that tau binds differently to different cell lines and can either promote or demote microtubule polymerization. However, the relative binding affinity of tau to the different  $\beta$ -tubulin isotypes present in different cell lines is completely unknown. Here, we study relative binding affinity of Tau repeat region R2 to neuronal specific tubulin isotypes  $\beta$ I,  $\beta$ IIb, and  $\beta$ III using molecular modelling approach. The order of binding energy of tau with tubulin is  $\beta$ III >  $\beta$ IIb >  $\beta$ I. Our strategy can be potentially adapted to understand differential binding affinity of tau towards  $\beta$ -tubulin isotypes present in other cell lines.

Tau is a microtubule-associated intrinsically disordered protein encoded by gene '*mapt*' located on chromosome 17<sup>1</sup>, which is abundantly expressed in the brain and neuronal tissues<sup>2,3</sup>. A total of 6 tau isoforms are found in the human central nervous system whose length varies from 352 to 441 residues<sup>4</sup>. Tau consists of the N-terminal projectile domain (residue 1–244) which is composed of the acidic and proline-rich region, and the C-terminal domain comprising residues 245–441 which consists of 4 repeat regions i.e. R1, R2, R3 and R4 (Fig. 1). The isoforms of tau mainly differ by the presence of either R3 or R4 repeats at the C-terminal domain<sup>5</sup>. The longest isoform of tau is observed in humans which comprises 4 repeats i.e. R1, R2, R3 and R4. Whereas, the shortest isoform has 3 repeats (R1, R2 and R3) which is reported in the fetus brain<sup>4,6</sup>. Figure 1A shows the structure of tau repeat R2 bound to the  $\beta/\alpha/\beta$  tubulin subunits in the recently released CryoEM model<sup>7</sup>. Hereafter, we shall refer to tau repeat R2 as 'TauR2'. These tau repeats prefer to bind at the exterior surface of microtubule (MT) and help in its stabilization (Fig. 1A) and also regulate MT polymerization<sup>5</sup>. Figure 1B shows domain organization in the tau structure and Fig. 1C shows the sequence of TauR2. It is well known that tau mainly helps in the assembly and stabilization of axonal MTs, which contributes to the proper functioning of neuronal cells<sup>8</sup>. However, recently it has been reported that the tau is not only a stabilizer of axonal MTs but it is also enriched on the labile domain of the MT to promote its assembly<sup>9</sup>. In various neurodegenerative diseases, tau detaches from the MTs and forms abnormal, fibrillar structures of insoluble aggregates due to post-translational modifications<sup>10,11</sup>.

Structure of full-length tau has not yet been solved by using X-ray crystallography due to its intrinsically disordered nature. Also, efforts to obtain a solution structure of complete tau using NMR techniques have failed<sup>12</sup>. Thus, the interaction of tau repeats with MT has been studied using various biochemical and biophysical techniques<sup>13–16</sup>. Further, Cryo-EM study shows discontinuous density of tau repeat along with each protofilament upon MT binding<sup>7</sup>. Hence, the interaction of a synthetically developed R1 and R2 repeats of tau with MT were examined. It is observed that R1 and R2 repeat of tau adapt the extended structures along the crest of protofilament, stabilizing the interface between tubulin dimers<sup>7</sup>.

MTs are made up of  $\alpha\beta$ -tubulin heterodimers<sup>17</sup>. In eukaryotes, seven  $\alpha$ -tubulin and nine  $\beta$ -tubulin isotypes have been reported which show tissue-specific expressions. For example,  $\beta$ I isotype is expressed in all cells,  $\beta$ II and  $\beta$ III isotype are predominantly expressed in brain and neuronal cells, and  $\beta$ VI is expressed in erythroid cells

Department of Biosciences and Bioengineering, Indian Institute of Technology Bombay, Powai, Mumbai, 400076, Maharashtra, India. Correspondence and requests for materials should be addressed to A.K. (email: [akunwar@iitb.ac.in](mailto:akunwar@iitb.ac.in))

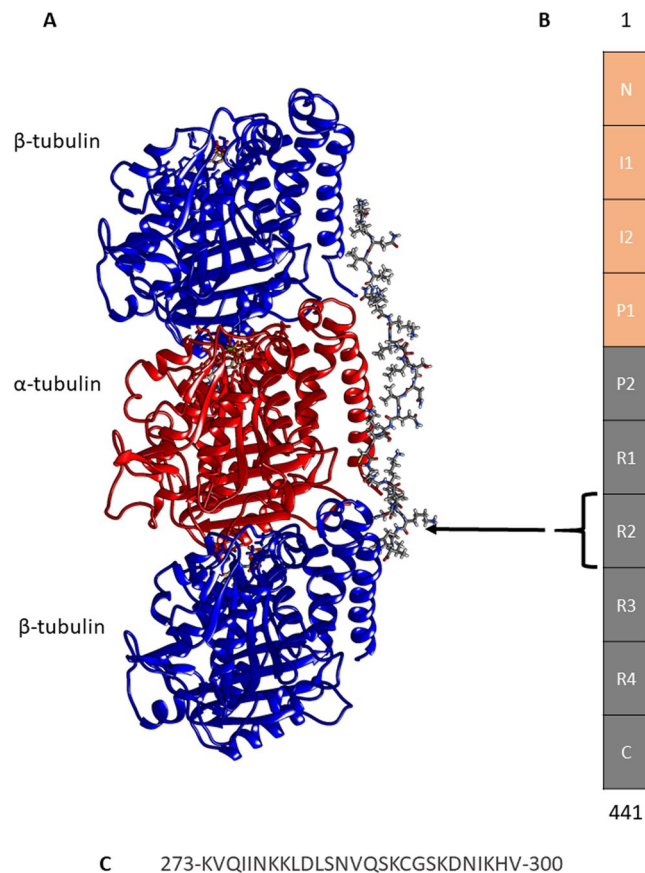


**Figure 1.** CryoEM Structure of tubulin subunits bound to TauR2. **(A)** tubulin subunits bound to TauR2 in CryoEM structure 6CVN.pdb. TauR2 domain binds at the outer surface of the MT. **(B)** Domain organization in tau, **(C)** sequence of TauR2.

and platelets<sup>18</sup>.  $\beta$ I plays important role in cell viability,  $\beta$ II is important for neurite growth and  $\beta$ III protects neurons against free radicals and reactive oxygen species<sup>19</sup>. It has been observed that all the  $\beta$ -tubulin isotypes share a significant homology except at their C-terminal tail region<sup>20–23</sup> which is highly flexible and disordered structure. The C-terminal tail regions in these isotypes protrude in the outward direction of the MTs where they interact with MAPs and regulate MT dynamics<sup>24,25</sup>.

It is well known that the composition of  $\beta$ -tubulin isotypes affect MT dynamic instability<sup>22,26</sup>, their interaction with motor proteins<sup>27</sup>, binding of anti-mitotic drugs<sup>20,21,28</sup> and different MAPs including tau<sup>29,30</sup>. These tubulin isotypes show tissue specific expression as their relative proportion varies significantly in different type of cells<sup>19,31,32</sup>. It is also known that tau binds differently to different cell lines and can either promote or demote microtubule polymerization<sup>33</sup>. However, the relative binding affinity of tau to the different  $\beta$ -tubulin isotypes present in different cell lines is completely unknown. Here, we study relative binding affinity of Tau repeat region R2 to neuronal specific  $\beta$ -tubulin isotypes namely  $\beta$ I,  $\beta$ IIb, and  $\beta$ III using molecular modeling approach.

## Results and Discussion

To gain insight into the detailed binding mode, relative binding affinity and inter-molecular interactions between neuronal specific tubulin isotypes and TauR2, we employ sequence analysis, homology modeling, MD simulations, and binding energy calculation.

**Sequence analysis and molecular modelling of tubulin isotypes.** The human  $\beta$ -tubulin isotypes show residue variations mostly at the carboxy-terminal tail region in multiple sequence alignment as shown in Fig. 2. The C-terminal tail regions of  $\beta$ I and  $\beta$ III tubulin isotypes are longer when compared with the  $\beta$ IIb isotype. The template  $\beta$ -tubulin sequence (6CVN; chain A) and human  $\beta$ IIb isotypes show 98.65% sequence identity. These sequence variations in the tubulin isotypes are known to regulate MT protofilament number and their stability<sup>34</sup>.

These sequences of  $\beta$ -tubulin isotypes were used to build three-dimensional homology models using 6CVN as the template structure. The tubulin isotypes  $\beta$ I,  $\beta$ IIb,  $\beta$ III were modeled using Modeller 9v20<sup>35</sup>. Best homology models for different tubulin isotypes were selected using DOPE score for chain A and chain C of  $\beta$  tubulins. The DOPE scores for the selected models of  $\beta$ I,  $\beta$ IIb and  $\beta$ III isotypes are given in Supplementary Table S1. The assessment of stereo-chemical properties of homology models was done using Ramachandran plot<sup>36,37</sup>.



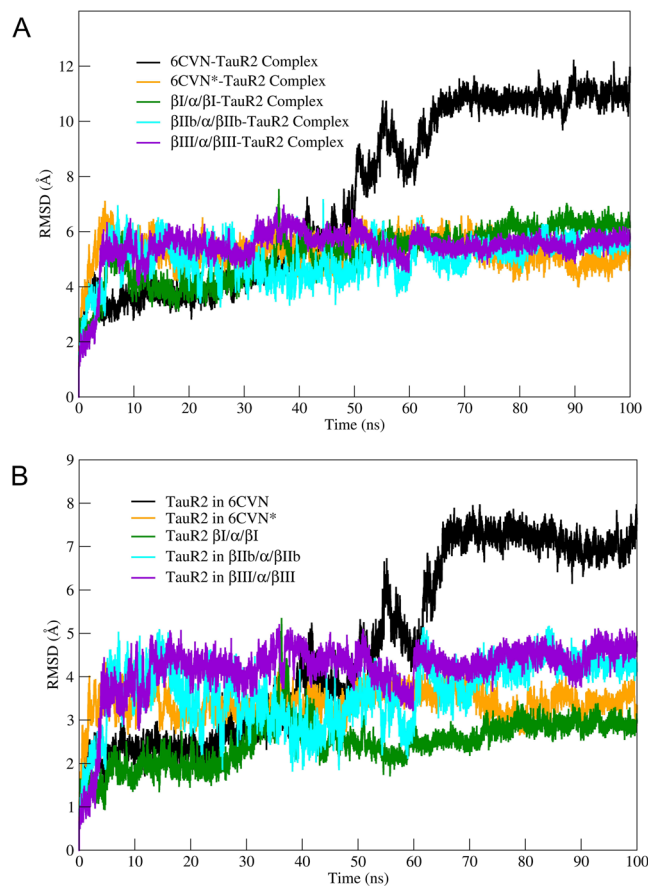


**Figure 3.** Stability of the tubulin-TauR2 complex and TauR2. **(A)** The Root mean square deviation values (RMSD) for tubulin-tauR2 complexes. RMSD values for 6CVN, 6CVN\*,  $\beta I/\alpha/\beta I$ ,  $\beta IIb/\alpha/\beta IIb$  and  $\beta III/\alpha/\beta III$  have been plotted in black, orange, green, cyan and violet respectively. **(B)** The Root mean square deviation values for TauR2 shown using same color Scheme as in **(A)**.

shows stable dynamics during simulation. The complex 6CVN-TauR2 is stabilized at higher RMSD mainly due to absence of C-tail region which highlights the importance of C-terminal tail in the stabilizing tubulin-TauR2 complex.

All above simulated systems are well equilibrated with the backbone RMSD value of  $\sim 3.5$  Å (Supplementary Fig. S2). The stable dynamics of all the simulated systems namely 6CVN-TauR2, 6CVN\*-TauR2,  $\beta I/\alpha/\beta I$ -TauR2,  $\beta IIb/\alpha/\beta IIb$ -TauR2 and  $\beta III/\alpha/\beta III$ -TauR2 are shown in Supplementary Movies S1–S5 respectively. To check the specificity of TauR2 towards tubulin subunits we replaced TauR2 with negative control polyA peptide of same length. Interestingly, our negative control system 6CVN\*-polyA complex shows the loose binding during the simulation due to weaker interactions of polyA peptide with tubulin subunits (Supplementary Movie S6), which establishes that TauR2 has specificity towards tubulin subunits.

**Residue fluctuations of tubulin subunits and TauR2.** The flexibility of tubulin trimers systems and TauR2 has been studied by plotting  $C\alpha$  fluctuations during the course of simulation. The RMSF for tubulin subunits and TauR2 is shown in Supplementary Fig. S3. TauR2 interacting residues from the H12 helix of  $\beta$ -tubulin and the C-terminal tail region (residue 400–451) show significant decrease in the fluctuations, as their free dynamics is arrested upon tau binding (Supplementary Fig. S3A,B). RMSF values for the tubulin  $\beta$ -subunits in the systems 6CVN\*,  $\beta IIb/\alpha/\beta IIb$  and  $\beta III/\alpha/\beta III$  are lesser than those of 6CVN and  $\beta I/\alpha/\beta I$  tubulin subunits (Supplementary Fig. S3B). The data also highlights the binding of TauR2 at the interdimer interface where it shows much lesser fluctuations while part of C-tail region which has no contact with TauR2 is highly flexible (Supplementary Fig. S3B). The H12 helix and C-terminal tail region contribute towards stronger binding by non-covalent interactions whose detailed analysis is given in the section ‘*Intermolecular interactions between tubulin and tau*’.

Further, we also analyzed the RMSF plot for TauR2 (Supplementary Fig. S3C) to analyze  $C\alpha$ -fluctuations of TauR2 for understanding its conformational behavior during MD simulations. It is observed that the TauR2 shows highest fluctuations at the N- and C-terminal region in the 6CVN, where the C-terminal tail region is absent (Supplementary Fig. S3C). Interestingly, residual fluctuations in TauR2 bound to  $\beta III/\alpha/\beta III$ -tau complex are less when compared to other tubulin-TauR2 complexes such as 6CVN\*-TauR2,  $\beta I/\alpha/\beta I$ -TauR2 and  $\beta IIb/\alpha/\beta IIb$ -TauR2 (Supplementary Fig. S3C). This also confirms that the C-terminal tail region of tubulin subunits plays an important role in the binding of TauR2.

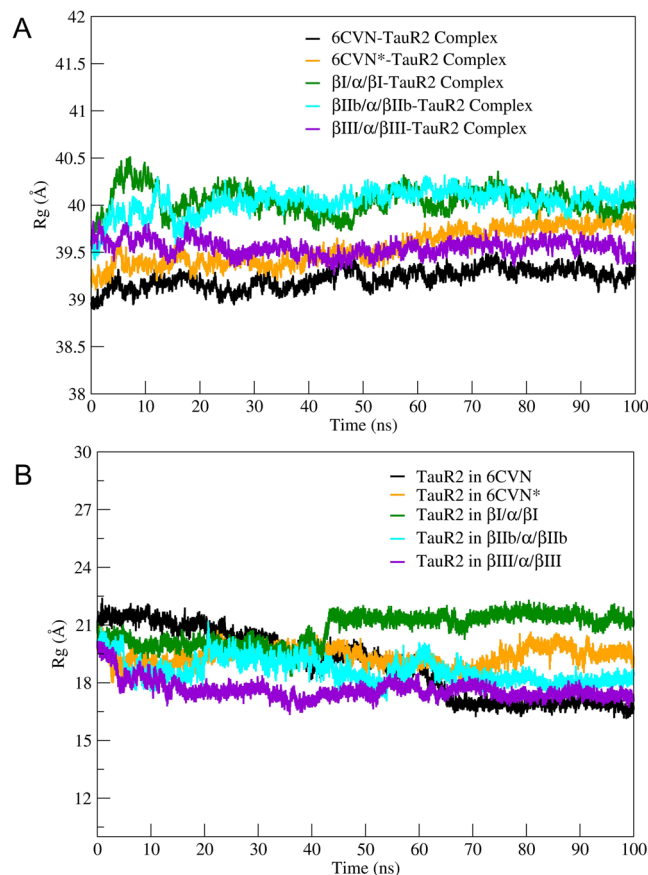


**Figure 4.** Radius of Gyration ( $R_g$ ) of different tubulin-TauR2 complexes and TauR2. (A)  $R_g$  of 6CVN-TauR2 (black), 6CVN\*-TauR2 (orange),  $\beta I/\alpha/\beta I$ -TauR2 (green),  $\beta IIb/\alpha/\beta IIb$ -TauR2 (cyan),  $\beta III/\alpha/\beta III$ -TauR2 (violet) (B)  $R_g$  for TauR2 in different tubulin-TauR2 complexes. Color scheme same as Fig. 3.

Overall, RMSF suggests the importance of H12-helix and C-terminal tail region in the binding of TauR2 and greater affinity of TauR2 towards  $\beta III$  tubulin isotypes. We further analyzed the compactness of all the tubulin-TauR2 systems using the radius of gyration ( $R_g$ ) as discussed in the next section.

**Compactness of tubulin-TauR2 complexes.** The radius of gyration ( $R_g$ ) indicates the level of compactness of the protein system which is helpful in getting an insight into the stability of the protein-protein complex. The tubulin-TauR2 complex shows the  $R_g$  values ranging from 38.8–40.5 Å (Fig. 4A). The complex  $\beta III/\alpha/\beta III$ -TauR2 expresses stable  $R_g$  value throughout the simulation whereas 6CVN-TauR2, 6CVN\*-TauR2,  $\beta I/\alpha/\beta I$ -TauR2,  $\beta IIb/\alpha/\beta IIb$ -TauR2 complexes show variations in their  $R_g$  values. Complex 6CVN-TauR2 shows less  $R_g$  values compared to other tubulin-TauR2 due to the absence of C-terminal tail region (Fig. 4A).

The  $R_g$  values of only TauR2 in different tubulin subunits are plotted in Fig. 4B for different tubulin-TauR2 complexes. The  $R_g$  values for TauR2 in case of 6CVN\*,  $\beta IIb/\alpha/\beta IIb$ , and  $\beta III/\alpha/\beta III$  complexes shows fluctuations between 17.5 to 20 Å except for  $\beta I/\alpha/\beta I$  complex (Fig. 4B). The  $\beta III$  tubulin subunits shows  $R_g$  value of ~18 Å and  $\beta I$  tubulin subunits have largest  $R_g$  value of 22.5 Å as shown in Fig. 4B.

However, 6CVN bound TauR2 shows continuous decrease in  $R_g$  values from 21.5 Å to 16.5 Å. This suggests the importance of C-terminal tail region in the stable binding of tau (Fig. 4B).

It is important to note that  $\beta III$  tubulin subunits (Supplementary Fig. S4) have  $R_g$  values similar to that of  $\beta III/\alpha/\beta III$ -TauR2 complex (Fig. 4A). This implies that the tubulin subunits composed of  $\beta III$  tubulin isotype are structurally stable after binding of TauR2.

Thus, our analysis of  $R_g$  for tubulin-TauR2 complexes, tubulin subunits and TauR2 highlights the stability of the  $\beta III/\alpha/\beta III$ -tau complex over other tubulin-TauR2 complexes and importance of the C-terminal tail region in the binding of TauR2.

To understand the exposure of the interface residues of tubulin subunits bound to the TauR2, we studied contact surface area (CSA) and solvent accessible surface area (SASA) using 'gmx sasa' tool of gromacs software<sup>42</sup>.

**Solvent accessible surface area for tubulin-TauR2 complexes.** The SASA and CSA describes the accessibility of a protein surface and binding interface to the solvent respectively. It is well known that, TauR2 binds to the MT exterior surface via C-terminal tail region<sup>7,43–46</sup>. Therefore, we first calculated the contact surface

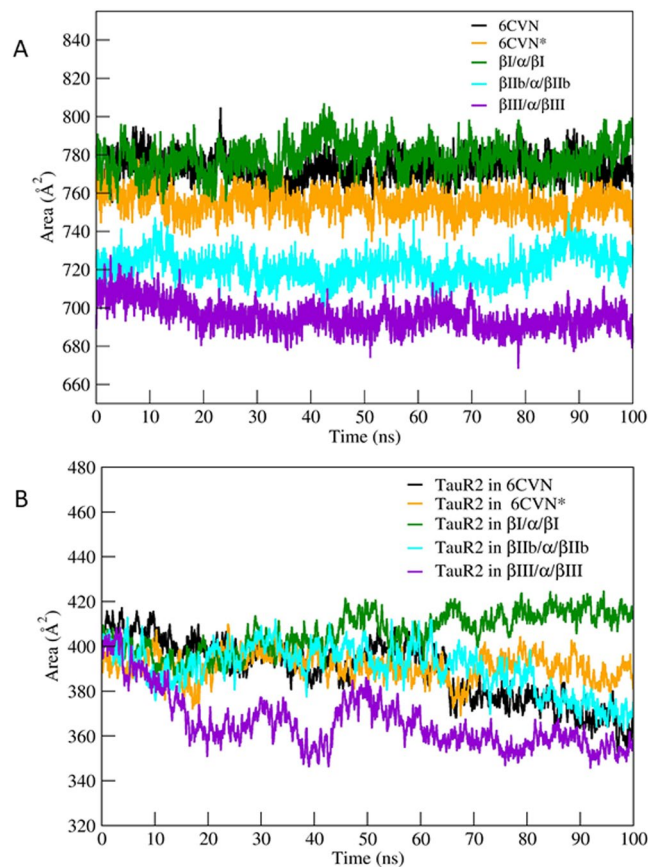


**Figure 5.** Contact surface area (CSA) and solvent accessible surface area (SASA) of different  $\beta/\alpha/\beta$ -tubulin subunits and TauR2. **(A)** CSA for different 6CVN-TauR2 (black), 6CVN\*-TauR2 (orange),  $\beta I/\alpha/\beta I$ -TauR2 (green),  $\beta IIb/\alpha/\beta IIb$ -TauR2 (cyan),  $\beta III/\alpha/\beta III$ -TauR2 (violet) complexes. **(B)** hydrophobic SASA for tubulin isotype bound TauR2. Color scheme same as Fig. 3.

area (CSA) of the interface where TauR2 binds, without considering flexible tail. The CSA of  $\beta III/\alpha/\beta III$  is very less when compared to other tubulin isotypes (Fig. 5A) which indicates tight binding of tauR2 to the  $\beta III/\alpha/\beta III$  tubulin subunits. The CSA is higher for  $\beta I/\alpha/\beta I$ -TauR2 complex indicates weaker binding of TauR2 to the  $\beta I/\alpha/\beta I$  tubulin subunits.

Furthermore, TauR2 bound to  $\beta III/\alpha/\beta III$  tubulin subunits shows least SASA which represents tight binding of TauR2 to the  $\beta III/\alpha/\beta III$  (Fig. 5B). Conversely, the TauR2 bound to  $\beta I/\alpha/\beta I$  tubulin subunits shows higher hydrophobic SASA which indicates that exposure of hydrophobic residues is responsible for disturbed contacts between tubulin and TauR2.

Further, SASA for tubulin subunits has also been plotted and shown in Supplementary Fig. S5. The SASA for 6CVN\*,  $\beta I/\alpha/\beta I$ ,  $\beta IIb/\alpha/\beta IIb$ ,  $\beta III/\alpha/\beta III$  shows higher SASA values between 4900–5400 Å<sup>2</sup> when compared to 6CVN-TauR2 (~4500 Å<sup>2</sup>) due to the presence of C-terminal tail (Supplementary Fig. S5).

To get detailed understanding of the atomic-level interaction between tubulin isotypes and TauR2, we further analyzed hydrogen bonds formed during the course of simulation and MD simulated end-structures obtained from simulations.

**Intermolecular interactions between tubulin and TauR2 in tubulin-TauR2 complexes.** In our MD simulations, the total number of hydrogen bonds formed between tubulin isotypes and TauR2 are calculated using in-built *gmx hbond* tool<sup>42</sup> with a cut-off value of 3.4 Å for H-bonds. All tubulin-TauR2 complexes show consistent H-bond formation throughout the simulation with the number of H-bonds roughly between 10 to 20 as shown in Supplementary Fig. S6. The details of hydrogen bonding interactions present between tubulin isotypes and TauR2 in the MD simulated end-structures are listed in Supplementary Table S4. The Supplementary Table S5 lists all the hydrophobic interactions participating in formation of stable tubulin-TauR2 complexes. Maximum number of electrostatic interactions are found in the  $\beta III/\alpha/\beta III$ -TauR2 complex when compared to other tubulin-TauR2 complexes (Supplementary Table S6). Additionally, it is observed that hydrophilic interactions also have a major contribution in stabilization of tubulin subunits by TauR2 (Supplementary Fig. S7).

To further understand the role of TauR2 in stabilizing tubulin subunits, we performed secondary structure analysis of TauR2 using DSSP.

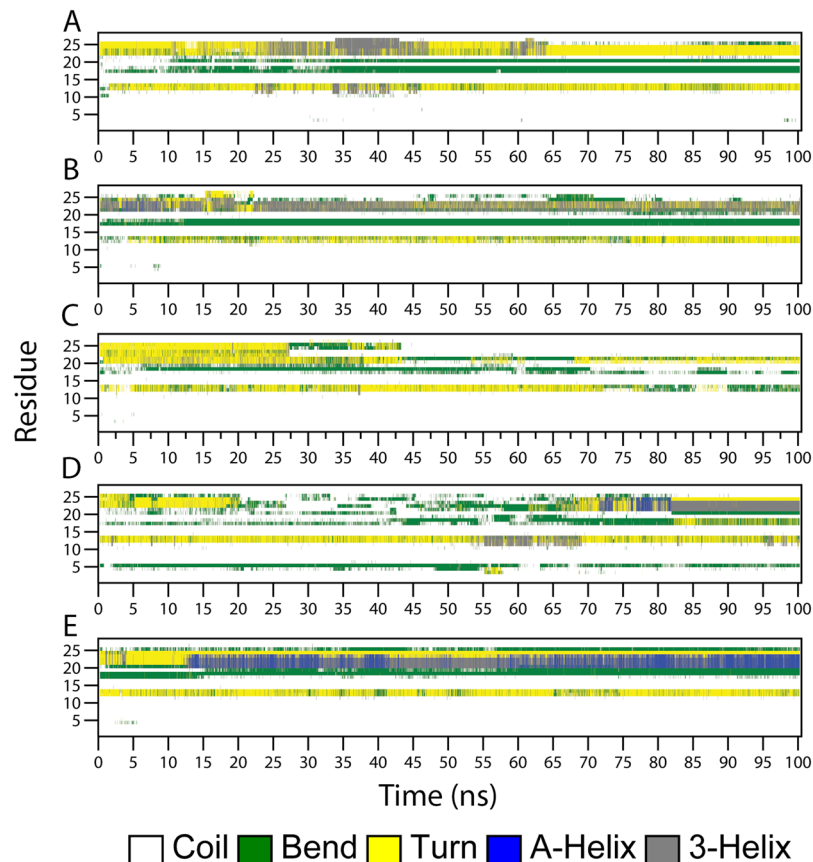


**Figure 6.** The secondary structure changes during MD simulation using DSSP for TauR2. Secondary structure changes observed in (A) 6CVN-TauR2 (B) 6CVN\*-TauR2 (C)  $\beta$ I/ $\alpha$ / $\beta$ I-TauR2, (D)  $\beta$ IIb/ $\alpha$ / $\beta$ IIb-TauR2 and (E)  $\beta$ III/ $\alpha$ / $\beta$ III-TauR2.

**Conformational changes in TauR2 upon tubulin binding.** Tau belongs to the class of intrinsically disordered proteins. Earlier experimental studies suggest that tau undergoes a conformational change from a disordered state to the ordered state upon binding to MT<sup>1,47–50</sup>. Therefore, we investigated the conformational changes in the secondary structure of TauR2 during MD simulations using DSSP program<sup>51</sup>. The conformational changes in the TauR2 upon binding to the tubulin subunits are shown in Fig. 6. TauR2 bound to 6CVN (Fig. 6A) and 6CVN\* (Fig. 6B) show the formation of short and transient  $3_{10}$ -helix during simulation which is not very consistent throughout the course of simulation. The TauR2 bound to  $\beta$ I/ $\alpha$ / $\beta$ I tubulin subunits does not show the formation of either  $\alpha$ -helix or  $3_{10}$ -helix as shown in Fig. 6C. The TauR2 in  $\beta$ IIb/ $\alpha$ / $\beta$ IIb-TauR2 complex exhibits the formation of short-lived  $\alpha$ -helix and  $3_{10}$ -helix as shown in Fig. 6D. The terminal region of TauR2 (residues Ser293-Val300) undergoes a conformational transition from turn to  $\alpha$ -helix as shown in Fig. 6E during simulation in  $\beta$ III/ $\alpha$ / $\beta$ III-TauR2 complex. We propose that, this conformational transition promotes the stable binding of TauR2 with the  $\beta$ III/ $\alpha$ / $\beta$ III tubulin subunits.

**Relative binding affinity of TauR2 towards different tubulin isoforms.** The relative binding affinity of TauR2 towards tubulin subunits ( $\beta$ / $\alpha$ / $\beta$ ) was analyzed by calculating the binding energy of 6CVN-tau, 6CVN\*-tau,  $\beta$ I/ $\alpha$ / $\beta$ I-tau,  $\beta$ IIb/ $\alpha$ / $\beta$ IIb-tau and  $\beta$ III/ $\alpha$ / $\beta$ III-tau complexes. The energy components governing the binding energy are listed in Table 1. The relative binding energy values observed for 6CVN-tau, 6CVN\*-tau,  $\beta$ I/ $\alpha$ / $\beta$ I-tau,  $\beta$ IIb/ $\alpha$ / $\beta$ IIb-tau and  $\beta$ III/ $\alpha$ / $\beta$ III-tau are  $-927.87 \pm 3.15$ ,  $-1331.15 \pm 3.19$ ,  $-1134.13 \pm 1.13$ ,  $-1365.22 \pm 2.26$  and  $-1404.7 \pm 1.84$  kcal/mol, respectively. The binding energy analysis reveals that, interactions of  $\beta$ III/ $\alpha$ / $\beta$ III-tau complex is most favorable while 6CVN-tau complex is least favorable (Table 1). Thus, it is interesting to note the significance of C-terminal tail of the tubulin subunits in the stable binding of the tau repeat R2. The order of binding energy of TauR2 for different tubulin-TauR2 complexes is  $\beta$ III/ $\alpha$ / $\beta$ III >  $\beta$ IIb/ $\alpha$ / $\beta$ IIb > 6CVN\* >  $\beta$ I/ $\alpha$ / $\beta$ I > 6CVN.

Binding energy calculations suggest that the electrostatic interactions are favorable for binding; the  $\beta$ III/ $\alpha$ / $\beta$ III and  $\beta$ IIb/ $\alpha$ / $\beta$ IIb tubulin subunit show least electrostatic energy in comparison to the 6CVN and  $\beta$ I/ $\alpha$ / $\beta$ I tubulin subunits as shown in Table 1. Thus, the electrostatic energy makes significant contributions in the binding of TauR2 to the tubulin isoforms particularly in  $\beta$ III/ $\alpha$ / $\beta$ III-TauR2 and  $\beta$ IIb/ $\alpha$ / $\beta$ IIb-TauR2 complexes. The  $\beta$ I/ $\alpha$ / $\beta$ I-TauR2 complex exhibits higher binding energy which is responsible for its weaker affinity for TauR2.

System	6CVN	6CVN*	$\beta I/\alpha/\beta I$	$\beta II/\alpha/\beta II$	$\beta III/\alpha/\beta III$
Vdw	$-97.25 \pm 0.55$	$-131.17 \pm 0.62$	$-133.38 \pm 0.69$	$-124.36 \pm 0.60$	$-125.24 \pm 0.59$
Elec	$-1232.33 \pm 3.43$	$-1534.36 \pm 3.12$	$-1423.07 \pm 2.77$	$-1659.30 \pm 4.68$	$-1768.65 \pm 2.77$
Polar	$413.98 \pm 4.73$	$349.43 \pm 4.18$	$439.27 \pm 2.95$	$433.79 \pm 4.13$	$505.14 \pm 2.92$
SASA	$-12.35 \pm 0.06$	$-15.12 \pm 0.07$	$-17.05 \pm 0.05$	$-15.66 \pm 0.06$	$-16.04 \pm 0.05$
Binding Energy	$-927.87 \pm 3.15$	$-1331.15 \pm 3.19$	$-1134.13 \pm 1.13$	$-1365.226 \pm 2.26$	$-1404.7 \pm 1.84$

**Table 1.** The Relative binding energy of the tubulin-TauR2 complexes calculated using MMPBSA. All energies are given in kcal/mol.

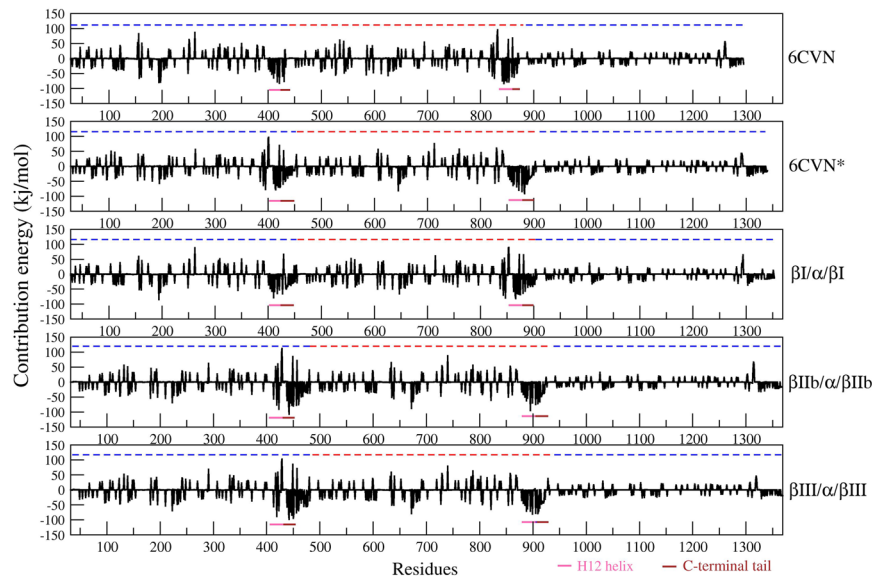


**Figure 7.** Residue decomposition energy of different tau-tubulin complexes. The H12 and C-terminal tail regions show highest energy contribution for the binding of TauR2 in 6CVN\*,  $\beta I/\alpha/\beta I$ ,  $\beta IIb/\alpha/\beta IIb$  and  $\beta III/\alpha/\beta III$  tubulin subunits except in case of 6CVN which does not have C-terminal tail region.

The  $\beta III/\alpha/\beta III$ -TauR2 and  $\beta IIb/\alpha/\beta IIb$ -TauR2 complexes exhibit relatively higher affinity towards TauR2 as revealed by their relative binding energy analysis. In addition, the contribution of the individual residues in the binding energy has been analyzed by calculating the decomposition energy for each residue. The decomposition energy analysis reveals maximum contribution of H12 helix and C-terminal tail of tubulin subunits in the TauR2 binding, compared to other residues (Fig. 7). In order to highlight the importance of the interacting residues between tubulin and TauR2, per-residue interactions energy was calculated for various pairs of interacting residues between tubulin and TauR2 (Supplementary Table S7). It was found that the residues from the H12-helices and C-terminal tail regions of  $\beta III/\alpha/\beta III$  complex shows maximum contribution to non-bonded contacts due to lowest energy from all pairs of interacting residues. This leads to the tight binding of the TauR2 to the  $\beta III/\alpha/\beta III$  tubulin.

Hence, our relative binding energy calculations further support the results obtained from the MD simulations that the TauR2 binds stronger to the  $\beta III/\alpha/\beta III$  tubulin isotype which is predominantly expressed in the neuronal cells and brain.

## Conclusion

There exists a large diversity of differently expressed  $\beta$ -tubulin isotypes distributed in the MT structure of different cells, which makes microtubules unique from one another in relative proportion of isotypes. The expression levels of  $\beta II$  and  $\beta III$  has been reported to be much higher in neuronal cells (i.e., 58% and 25% respectively)<sup>33</sup>. In the present study, we investigated the binding mode and interaction of neuronal specific tubulin isotypes with TauR2 using molecular modeling approach.

Our MD simulation results show a stable complex formation in between different tubulin isotypes and TauR2 which are mainly mediated by the interactions of H12 helix and C-terminal tail region of the  $\alpha\beta$  tubulin isotypes with TauR2. Our results suggest that tau shows differential binding affinity towards various  $\beta$ -tubulin isotypes. The order of binding affinity of TauR2 with  $\beta$  tubulin isotypes is  $\beta III > \beta IIb > \beta I$ . Thus, we find that TauR2 has greater affinity towards  $\beta$  tubulin isotypes which are abundantly expressed in neuronal cells i.e.  $\beta III$  and  $\beta IIb$ . Our strategy can be potentially used to understand differential binding affinity of tau towards  $\beta$  tubulin isotypes present in other cell lines. We hope that knowledge of precise molecular origin of differential binding affinity of tau with  $\beta$  tubulin isotypes present different cell types will pave the way for developing effective treatments against tau related disorders.

## Methodology

**Sequence analysis and homology modeling of tubulin isotypes.** High-resolution Cryo-EM structure of  $\beta/\alpha/\beta$ -tubulin bound with TauR2 (PDB ID: 6CVN.pdb)<sup>7</sup> was used as a template structure to build different tubulin isotype-TauR2 complexes, namely  $\beta I/\alpha/\beta I$ -TauR2,  $\beta IIb/\alpha/\beta IIb$ -TauR2 and  $\beta III/\alpha/\beta III$ -TauR2. The template structure 6CVN.pdb is from *Sus scrofa* source with the resolution of 3.9 Å<sup>7</sup>. The CryoEM structure '6CVN.pdb' has  $\beta/\alpha/\beta$ -tubulin subunit bound with TauR2. The template structure (6CVN.pdb) does not have C-terminal tail, therefore we build the tail region using the Modeller 9v20 software. Hereafter, we refer to template structure with modeled C-terminal tail region as 6CVN\*.

We used 6CVN.pdb as template structure for homology modeling of different human tubulin isotypes as it shows maximum identity with human  $\beta I$ ,  $\beta IIb$  and  $\beta III$  tubulin isotypes having uniprot IDs Q9H4B7, Q9BVA1 and Q136509 respectively. Sequence similarities between different tubulin isotypes were studied using 'Clustal Omega' tool<sup>52</sup>. The sequence analysis shows that the most residue variations are mainly at the C-terminal tail region compared to the other region.

Homology models of  $\beta I$ ,  $\beta IIb$ ,  $\beta III$  tubulin isotypes were generated using Modeller 9v20<sup>35</sup>. The least energy models of  $\beta$ -tubulin were selected based on their discrete optimized potential energy (DOPE) score. The three dimensional stereo-chemical quality of these homology models were evaluated using Ramachandran plot through RAMPAGE<sup>53</sup>. The quality of the homology models were further checked using GMQE score<sup>38</sup>, Verify3D<sup>39</sup> and ERRAT score<sup>40</sup>. The selected models were further used to build different tubulin isotype-TauR2 complexes such as  $\beta I/\alpha/\beta I$ -TauR2,  $\beta IIb/\alpha/\beta IIb$ -TauR2 and  $\beta III/\alpha/\beta III$ -TauR2 using refined template structure i.e. 6CVN\*-TauR2. These models (6CVN-TauR2, 6CVN\*-TauR2,  $\beta I/\alpha/\beta I$ -TauR2,  $\beta IIb/\alpha/\beta IIb$ -TauR2 and  $\beta III/\alpha/\beta III$ -TauR2) were subjected for energy minimization using Steepest Descent and Conjugate Gradient methods using Gromacs 2018.1<sup>41</sup>. These minimized models were used as a starting structure for molecular dynamics simulations to understand the binding mode and binding affinity of TauR2 towards different tubulin isotypes.

**Molecular dynamics simulations of tubulin-TauR2 complexes.** All atom explicit molecular dynamics (MD) simulations were performed on the tubulin-TauR2 complexes (i.e. 6CVN-TauR2, 6CVN\*-tau,  $\beta I/\alpha/\beta I$ -TauR2,  $\beta IIb/\alpha/\beta IIb$ -TauR2 and  $\beta III/\alpha/\beta III$ -TauR2) using GROMACS 2018.1<sup>41,42</sup>. The 'Amber99SB-ILDN' force field<sup>54</sup> was used for simulation of above-mentioned tubulin-TauR2 complexes. The force field parameter for the GDP and GTP molecules were taken from the amber parameter database<sup>55,56</sup>. The 'xleap' module of AmberTools was used to generate topologies and starting structure for all tubulin-TauR2 complexes<sup>57</sup>. These tubulin-TauR2 complexes were placed at the centre of the box with a distance of 15 Å from the wall surrounded by TIP3P water molecules with periodic boundary condition. The complexes were neutralized by adding appropriate number of required counter ions. The topology files generated using xleap module of AmberTools were converted to Gromacs topology files format using the ParmEd tool<sup>58</sup>. Energy minimization was performed in two steps - steepest descent algorithm was used for first 50,000 steps which was followed by 50000 steps using the conjugate gradient method<sup>42</sup>. The energy minimized systems were further equilibrated using canonical ensemble (NVT) followed by isothermal-isobaric ensemble (NPT). In the NVT equilibration, systems were heated to 300 K using V-rescale, a modified Berendsen thermostat<sup>42</sup> for 1 ns. In NPT, all these heated systems were equilibrated using the Parrinello-Rahman barostat for 1 ns to maintain constant pressure of 1 bar. The unrestrained production MD simulations were performed for 100 ns over all the tubulin-TauR2 complexes using parameters discussed in our earlier study<sup>59</sup>. The long range electrostatic interactions were treated with particle mesh Ewald (PME) method<sup>60,61</sup> and covalent bonds involving H-atoms were constrained using the 'LINCS' algorithm<sup>62</sup>. The time step for integration was set to 2 fs during the MD simulation. The convergence of our simulations for different tubulin-TauR2 complexes was examined using potential energy and backbone RMSD values.

We also performed all atom MD simulation on three additional systems i.e. 6CVN\* (without tau), free tau and 6CVN\*-polyA (as negative control) having 27 amino acids residues using same simulation protocols.

MD simulation trajectories were further analyzed by using the inbuilt tools in GROMACS 2018.1<sup>41,42</sup>. The secondary structure changes during MD simulation were studied using the dictionary of secondary structure of protein (DSSP) tool<sup>51</sup>. The simulation movies were generated using the visual molecular dynamics (VMD) software<sup>63</sup> and images were generated using the Biovia Discovery studio visualizer<sup>64</sup> and Chimera software<sup>65</sup>.

**Calculations of contact surface area for tubulin-TauR2 complexes.** The SASA denotes the degree of hydration of a biomolecule which is helpful to quantify its stability in the aqueous medium. The C-terminal tail of the tubulin is highly dynamic, and it affects the overall hydrophobic SASA. Therefore, interface of tubulin trimer and TauR2 has been selected for the calculating the precise contact surface area. The in-built gromacs tool 'gmx sasa'<sup>66</sup> was used to calculate the SASA. In addition, SASA is also calculated for the tubulin subunits and the TauR2.

**Binding affinity of TauR2 towards different tubulin isotypes.** The binding affinity between different tubulin isotypes and TauR2 was explored by performing relative binding energy calculation similar to earlier studies<sup>67-69</sup>. The stable region of the trajectory observed in between 70 ns to 100 ns and hence we extracted 70-100 ns trajectory to perform the binding energy calculations for all the tubulin-TauR2 complexes. The tool 'g\_mmpbsa' v1.6 was used to calculate binding energy using MM/PBSA approach<sup>70</sup> implemented in gromacs 2018.1. The parameters for binding energy calculations were taken from the earlier similar studies<sup>59,69,71-73</sup>. The binding energy ( $\Delta G_{bind}$ ) of tubulin and TauR2 was calculated by using the following Eq. (1),

$$\Delta G_{bind} = \Delta G_{tubulin-TauR2} - (\Delta G_{tubulin} + \Delta G_{TauR2}) \quad (1)$$

Where, the  $\Delta G_{\text{tubulin-TauR2}}$ ,  $\Delta G_{\text{tubulin}}$  and  $\Delta G_{\text{TauR2}}$  denote the average free energies of the complex (tubulin-TauR2), receptor (tubulin) and ligand (TauR2), respectively. The calculation of entropic contribution to binding energy is computationally expensive for larger biomolecular complexes and hence it is omitted as similar to previous studies<sup>20,21,74–76</sup>.

## Data Availability

All data generated or analysed during this study are included in this published article (and its Supplementary Information files).

## References

- Melo, A. M. *et al.* A functional role for intrinsic disorder in the tau-tubulin complex. *Proc. Natl. Acad. Sci.* **113**, 14336–14341 (2016).
- Butner, K. A. & Kirschner, M. W. Tau Protein Binds to Microtubules through. *J. Cell Biol.* **115**, 717–730 (1991).
- Guo, T., Noble, W. & Hanger, D. P. Roles of tau protein in health and disease. *Acta Neuropathol.* **133**, 665–704 (2017).
- Liu, F. & Gong, C.-X. Tau exon 10 alternative splicing and tauopathies. *Mol. Neurodegener.* **3**, 8 (2008).
- Buée, L., Bussièrè, T., Buée-Scherrer, V., Delacourte, A. & Hof, P. R. Tau protein isoforms, phosphorylation and role in neurodegenerative disorders. *Brain Res. Rev.* **33**, 95–130 (2000).
- Kolarova, M., García-Sierra, F., Bartos, A., Ricny, J. & Ripova, D. Structure and Pathology of Tau Protein in Alzheimer Disease. *Int. J. Alzheimers. Dis.* **2012**, 1–13 (2012).
- Kellogg, E. H. *et al.* Near-atomic model of microtubule-tau interactions. *Science (80-)*. **1780**, eaat1780 (2018).
- Jebarupa, B., Muralidharan, M., Arun, A., Mandal, A. K. & Mitra, G. Conformational heterogeneity of tau: Implication on intrinsic disorder, acid stability and fibrillation in Alzheimer's disease. *Biophys. Chem.* **241**, 27–37 (2018).
- Qiang, L. *et al.* Tau Does Not Stabilize Axonal Microtubules but Rather Enables Them to Have Long Labile Domains. *Curr. Biol.* **28**, 2181–2189.e4 (2018).
- Brettschneider, J. *et al.* TDP-43 pathology and neuronal loss in amyotrophic lateral sclerosis spinal cord. *Acta Neuropathol.* **128**, 423–437 (2014).
- Gao, Y.-L. *et al.* Tau in neurodegenerative disease. *Ann. Transl. Med.* **6**, 175–175 (2018).
- Friedhoff, P., von Bergen, M., Mandelkow, E.-M. & Mandelkow, E. Structure of tau protein and assembly into paired helical filaments. *Biochim. Biophys. Acta - Mol. Basis Dis.* **1502**, 122–132 (2000).
- Kellogg, E. H. *et al.* Near-atomic model of microtubule-tau interactions. *Science (80-)*. eaat1780, <https://doi.org/10.1126/science.aat1780> (2018).
- Kadavath, H. *et al.* The Binding Mode of a Tau Peptide with Tubulin. *Angew. Chemie Int. Ed.* **57**, 3246–3250 (2018).
- Panda, D., Samuel, J. C., Massie, M., Feinstein, S. C. & Wilson, L. Differential regulation of microtubule dynamics by three- and four-repeat tau: Implications for the onset of neurodegenerative disease. *Proc. Natl. Acad. Sci.* **100**, 9548–9553 (2003).
- Panda, D., Goode, B. L., Feinstein, S. C. & Wilson, L. Kinetic Stabilization of Microtubule Dynamics at Steady State by Tau and Microtubule-Binding Domains of Tau. *Biochemistry* **34**, 11117–11127 (1995).
- Ludueña, R. F. A Hypothesis on the Origin and Evolution of Tubulin. *International Review of Cell and Molecular Biology* **302**, (Elsevier, 2013).
- Ludueña, R. F. & Banerjee, A. The Isoforms of Tubulin. in *The Role of Microtubules in Cell Biology, Neurobiology, and Oncology* 123–175, [https://doi.org/10.1007/978-1-59745-336-3\\_6](https://doi.org/10.1007/978-1-59745-336-3_6) (Humana Press, 2008).
- Guo, J., Walss-Bass, C. & Ludueña, R. F. The beta isoforms of tubulin in neuronal differentiation. *Cytoskeleton (Hoboken)*. **67**, 431–441 (2010).
- Kumbhar, B. V., Borogaon, A., Panda, D. & Kunwar, A. Exploring the Origin of Differential Binding Affinities of Human Tubulin Isoforms  $\alpha$ II,  $\alpha$ III and  $\alpha$ IV for DAMA-Colchicine Using Homology Modelling, Molecular Docking and Molecular Dynamics Simulations. *PLoS One* **11**, e0156048 (2016).
- Kumbhar, B. V., Panda, D. & Kunwar, A. Interaction of microtubule depolymerizing agent indanocine with different human  $\alpha$ 3 tubulin isoforms. 1–20, <https://doi.org/10.1371/journal.pone.0194934> (2018).
- Pamula, M. C., Ti, S.-C. & Kapoor, T. M. The structured core of human  $\beta$  tubulin confers isotype-specific polymerization properties. *J. Cell Biol.* **213**, 425–433 (2016).
- Fees, C. P., Aiken, J., O'Toole, E. T., Giddings, T. H. & Moore, J. K. The negatively charged carboxy-terminal tail of  $\beta$ -tubulin promotes proper chromosome segregation. *Mol. Biol. Cell* **27**, 1786–1796 (2016).
- Roll-Mecak, A. Intrinsically disordered tubulin tails: complex tuners of microtubule functions? *Semin. Cell Dev. Biol.* **37**, 11–9 (2015).
- Janke, C. The tubulin code: Molecular components, readout mechanisms, functions. *J. Cell Biol.* **206**, 461–472 (2014).
- Panda, D., Miller, H. P., Banerjee, A., Ludueña, R. F. & Wilson, L. Microtubule dynamics *in vitro* are regulated by the tubulin isotype composition. *Proc. Natl. Acad. Sci.* **91**, 11358–11362 (1994).
- Shojania Feizabadi, M. *et al.* Microtubule C-Terminal Tails Can Change Characteristics of Motor Force Production. *Traffic* **16**, 1075–1087 (2015).
- Banerjee, A. & Ludueña, R. F. Kinetics of colchicine binding to purified beta-tubulin isoforms from bovine brain. *J. Biol. Chem.* **267**, 13335–13339 (1992).
- Cowan, N. J., Lewis, S. A. & Gu, W. & Buraoyne, R. D. Tubulin Isoforms and Their Interaction with Microtubule Associated Proteins. *Protoplasma* **145**, 6–111 (1988).
- Murphy, D. B. Purification of Tubulin and Tau from Chicken Erythrocytes: Tubulin Isoforms and Mechanisms of Microtubule Assembly. *Methods Enzymol.* **196**, 235–246 (1991).
- Ludueña, R. F. Are Tubulin Isoforms Functionally Significant. *Mol. Biol. Cell* **4**, 445–457 (1993).
- Vemu, A., Atherton, J., Spector, J. O., Moores, C. A. & Roll-Mecak, A. Tubulin isoform composition tunes microtubule dynamics. *Mol. Biol. Cell* **28**, 3564–3572 (2017).
- Feizabadi, M. S., Hernandez, M. A. V., Breslin, J. B. & Akintola, I. I. The regulatory effect of Tau protein on polymerization of MCF7 microtubules *in vitro*. *Biochem. Biophys. Reports* **17**, 151–156 (2019).
- Ti, S.-C., Alushin, G. M. & Kapoor, T. M. Human  $\beta$ -Tubulin Isoforms Can Regulate Microtubule Protofilament Number and Stability. *Dev. Cell*, <https://doi.org/10.1016/j.devcel.2018.08.014> (2018).
- Webb, B. & Sali, A. Comparative Protein Structure Modeling Using MODELLER. In *Current Protocols in Bioinformatics* **86**, 5.6.1–5.6.37 (John Wiley & Sons, Inc., 2016).
- Lovell, S. C. *et al.* Structure validation by C $\alpha$  geometry: phi,psi and Cbeta deviation. *Proteins* **50**, 437–50 (2003).
- Ramachandran, G. N., ramakrishnan, C. & sasisekharan, V. Stereochemistry of polypeptide chain configurations. *J. Mol. Biol.* **7**, 95–9 (1963).
- Biasini, M. *et al.* SWISS-MODEL: Modelling protein tertiary and quaternary structure using evolutionary information. *Nucleic Acids Res.* **42**, W252–W258 (2014).
- Eisenberg, D., Lüthy, R. & Bowie, J. U. [20] VERIFY3D: Assessment of protein models with three-dimensional profiles. *Methods Enzymol.* **277**, 396–404 (1997).

40. Colovos, C. & Yeates, T. O. Verification of protein structures: patterns of nonbonded atomic interactions. *Protein Sci.* **2**, 1511–9 (1993).
41. Van Der Spoel, D. *et al.* GROMACS: fast, flexible, and free. *J Comput Chem* **26**, 1701–1718 (2005).
42. Berendsen, H. J. C., van der Spoel, D. & van Drunen, R. GROMACS: A message-passing parallel molecular dynamics implementation. *Comput. Phys. Commun.* **91**, 43–56 (1995).
43. Kar, S., Fan, J., Smith, M. J., Goedert, M. & Amos, L. A. Repeat motifs of tau bind to the insides of microtubules in the absence of taxol. *EMBO J.* **22**, 70–7 (2003).
44. Chau, M.-F. *et al.* The Microtubule-Associated Protein Tau Cross-Links to Two Distinct Sites on Each  $\alpha$  and  $\beta$  Tubulin Monomer via Separate Domains †. *Biochemistry* **37**, 17692–17703 (1998).
45. Al-Bassam, J., Ozer, R. S., Safer, D., Halpain, S. & Milligan, R. A. MAP2 and tau bind longitudinally along the outer ridges of microtubule protofilaments. *J. Cell Biol.* **157**, 1187–1196 (2002).
46. Santarella, R. A. *et al.* Surface-decoration of microtubules by human tau. *J. Mol. Biol.* **339**, 539–553 (2004).
47. Luo, Y., Ma, B., Nussinov, R. & Wei, G. Structural Insight into Tau Protein's Paradox of Intrinsically Disordered Behavior, Self-Acetylation Activity, and Aggregation. *J. Phys. Chem. Lett.* **5**, 3026–3031 (2014).
48. Avila, J. *et al.* Tau Structures. *Front. Aging Neurosci.* **8**, 262 (2016).
49. Fischer, D. *et al.* Structural and microtubule binding properties of tau mutants of frontotemporal dementias. *Biochemistry* **46**, 2574–2582 (2007).
50. Ma, B., Wei, G., Zhen, J. & Nussinov, R. Dancing with Strings: The Conformational Dynamics of VQIXXK Motifs within Tau Protein in Monomer, Fibril and Hyper-Phosphorylated Filament States. *Biophys. J.* **110**, 553a–554a (2016).
51. Kabsch, W. & Sander, C. Dictionary of protein secondary structure: pattern recognition of hydrogen-bonded and geometrical features. *Biopolymers* **22**, 2577–2637 (1983).
52. Sievers, F. *et al.* Fast, scalable generation of high-quality protein multiple sequence alignments using Clustal Omega. *Mol. Syst. Biol.* **7**, 539–539 (2014).
53. Rampage. Available at, <http://mordred.bioc.cam.ac.uk/rapper/rampage.php>.
54. Lindorff-Larsen, K. *et al.* Improved side-chain torsion potentials for the Amber ff99SB protein force field. *Proteins Struct. Funct. Bioinforma.* **78**, NA-NA (2010).
55. Meagher, K. L., Redman, L. T. & Carlson, H. A. Development of polyphosphate parameters for use with the AMBER force field. *J. Comput. Chem.* **24**, 1016–25 (2003).
56. Allnér, O., Nilsson, L. & Villa, A. Magnesium Ion-Water Coordination and Exchange in Biomolecular Simulations. *J. Chem. Theory Comput.* **8**, 1493–502 (2012).
57. Case, D. A. *et al.* AMBER 12; University of California: San Francisco, 2012. (2012).
58. ParmEd tool. Available at, <http://parmed.github.io/ParmEd/html/index.html>.
59. Bhandare, V. V. & Ramaswamy, A. The proteinopathy of D169G and K263E mutants at the RNA Recognition Motif (RRM) domain of tar DNA-binding protein (tdp43) causing neurological disorders: A computational study. *J. Biomol. Struct. Dyn.*, <https://doi.org/10.1080/07391102.2017.1310670> (2017).
60. Essmann, U. *et al.* A smooth particle mesh Ewald method. *J. Chem. Phys.* **103**, 8577–8593 (1995).
61. Darden, T., York, D. & Pedersen, L. Particle mesh Ewald: An  $N \cdot \log(N)$  method for Ewald sums in large systems. *J. Chem. Phys.* **98**, 10089–10092 (1993).
62. Hess, B., Bekker, H., Berendsen, H. J. C. & Fraaije, J. G. LINCS: A Linear Constraint Solver for Molecular Simulations. *Artic./Lett. to Ed.* **18**, 1463–1472 (1977).
63. Humphrey, W., Dalke, A. & Schulten, K. VMD: visual molecular dynamics. *J Mol Graph* **14**(27–28), 33–38 (1996).
64. Biovia Discovery studio Visualizer (2017).
65. Pettersen, E. F. *et al.* UCSF Chimera—a visualization system for exploratory research and analysis. *J. Comput. Chem.* **25**, 1605–1612 (2004).
66. Hess, B., van Der Spoel, D. & Lindahl, E. Gromacs user manual version 4.5. 4. *Univ. Groningen, Netherl.* (2010).
67. Wong, S., Amaro, R. E. & McCammon, J. A. MM-PBSA Captures Key Role of Intercalating Water Molecules at a Protein–Protein Interface. *J. Chem. Theory Comput.* **5**, 422–429 (2009).
68. Aldeghi, M., Bodkin, M. J., Knapp, S. & Biggin, P. C. Statistical Analysis on the Performance of Molecular Mechanics Poisson–Boltzmann Surface Area versus Absolute Binding Free Energy Calculations: Bromodomains as a Case Study. *J. Chem. Inf. Model.* **57**, 2203–2221 (2017).
69. Kant, V., Vijayakumar, S., Sahoo, G. C., Chaudhery, S. S. & Das, P. In-silico screening and validation of high-affinity tetra-peptide inhibitor of Leishmania donovani O-acetyl serine sulfhydrylase (OASS). *J. Biomol. Struct. Dyn.* **1–14**, <https://doi.org/10.1080/07391102.2018.1429315> (2018).
70. Kumari, R., Kumar, R. & Lynn, A. g\_mmpbsa—a GROMACS tool for high-throughput MM-PBSA calculations. *J Chem Inf Model* **54**, 1951–1962 (2014).
71. Bhandare, V. V. & Ramaswamy, A. Structural dynamics of human argonaute2 and its interaction with siRNAs designed to target mutant tdp43. *Adv. Bioinformatics* **2016** (2016).
72. Kumari, R., Kumar, R. & Lynn, A. g\_mmpbsa-A GROMACS Tool for High-Throughput MM-PBSA Calculations. *J. Chem. Inf. Model.* **54**, 1951–1962 (2014).
73. Cavuturu, B. M., Bhandare, V. V., Ramaswamy, A. & Arumugam, N. Molecular dynamics of interaction of Sesamin and related compounds with the cancer marker  $\beta$ -catenin: an in silico study. *J. Biomol. Struct. Dyn.*, <https://doi.org/10.1080/07391102.2018.1442250> (2018).
74. Guo, W. *et al.* An ALS-associated mutation affecting TDP-43 enhances protein aggregation, fibril formation and neurotoxicity. *Nat Struct Mol Biol* **18**, 822–830.
75. Wang, C., Greene, D., Xiao, L., Qi, R. & Luo, R. Recent Developments and Applications of the MMPBSA Method. *Front. Mol. Biosci.* **4**, 87 (2017).
76. Miller, B. R. *et al.* MMPBSA.py: An Efficient Program for End-State Free Energy Calculations. *J. Chem. Theory Comput.* **8**, 3314–21 (2012).

## Acknowledgements

VVB is thankful to the Indian Institute of Technology Bombay for Institute Post-Doctoral Fellowship. A.K. is thankful to the Department of Biotechnology, Government of India, Pilot Project Grants (No. 6242-P12/RGCB/PMD/DBT/AMBK/2015) for young investigators in cancer biology.

## Author Contributions

V.B., B.K. and A.K. designed research, V.B. performed research, V.B. analyzed data, and all authors wrote the manuscript.

## Additional Information

**Supplementary information** accompanies this paper at <https://doi.org/10.1038/s41598-019-47249-7>.

**Competing Interests:** The authors declare no competing interests.

**Publisher's note:** Springer Nature remains neutral with regard to jurisdictional claims in published maps and institutional affiliations.



**Open Access** This article is licensed under a Creative Commons Attribution 4.0 International License, which permits use, sharing, adaptation, distribution and reproduction in any medium or format, as long as you give appropriate credit to the original author(s) and the source, provide a link to the Creative Commons license, and indicate if changes were made. The images or other third party material in this article are included in the article's Creative Commons license, unless indicated otherwise in a credit line to the material. If material is not included in the article's Creative Commons license and your intended use is not permitted by statutory regulation or exceeds the permitted use, you will need to obtain permission directly from the copyright holder. To view a copy of this license, visit <http://creativecommons.org/licenses/by/4.0/>.

© The Author(s) 2019